Vol. 44 — N° 3 09 20 P. 485 – 500

GEOSTANDARDS and GEOANALYTICAL RESEARCH

A Potential New Chalcopyrite Reference Material for Secondary Ion Mass Spectrometry Sulfur Isotope Ratio Analysis

Rucao **Li** (1, 2), Xiao-Ping **Xia** (1)*, Huayong **Chen** (2), Nanping **Wu** (3), Taiping **Zhao** (2), Chunkit **Lai** (4), Qing **Yang** (1) and Yanqiang **Zhang** (1)

(1) State Key Laboratory of Isotope Geochemistry, Guangzhou Institute of Geochemistry, Chinese Academy of Sciences, Guangzhou, 510604, China
(2) Key Laboratory of Mineralogy and Metallogeny, Guangzhou Institute of Geochemistry, Chinese Academy of Sciences, Guangzhou, 510604, China
(3) Department of Geology, University of Maryland, College Park, MD, 20740, USA
(4) Faculty of Science, University Brunei Darussalam, Gadong, BE1410, Brunei Darussalam
* Corresponding author. e-mail: xpxia@gig.ac.cn

Chalcopyrite is an important sulfide mineral in many types of ore deposits, but matrix-matched chalcopyrite reference materials for microanalysis are lacking. A new natural chalcopyrite-bearing specimen (HTS4-6) was analysed in this study to investigate its potential as a reference material for microbeam sulfur isotope ratio measurement. Detailed textural examination and major element determination showed that the HTS4-6 chalcopyrite grains have no growth rim or zoning. A total of 607 sulfur isotope ratio spot measurements with secondary ion mass spectrometry (SIMS) conducted on the cruciform sections, and over 120 randomly selected grains yielded highly consistent sulfur isotope ratio. The intermediate measurement precision for four measurement sessions of the $^{34}S/^{32}S$ measurement results was better than 0.39‰ (2*s*). Randomly selected chalcopyrite grains of HTS4-6 were further analysed by LA-MC-ICP-MS, which gave a mean $\delta^{34}S$ value of +0.58 ± 0.38‰ (2*s*, *n* = 95). The maximum variance (expressed as intermediate precision from SIMS and LA-MC-ICP-MS measurements) is not worse than 0.39‰ (the SIMS value), indicating that HTS4-6 chalcopyrite is a potential reference material for *in situ* microbeam sulfur isotope measurements. The mean $\delta^{34}S$ value determined by gas source isotope ratio mass spectrometry (GS-IRMS) is +0.63 ± 0.16‰ (2*s*, *n* = 23), consistent with that derived by LA-MC-ICP-MS, and can represent the recommended value for this potential reference material.

Keywords: chalcopyrite, reference material, HTS4-6, sulfur isotopes, secondary ion mass spectrometry, SIMS.

Received 05 Jul 19 – Accepted 09 Mar 20

Chalcopyrite is a major sulfide mineral in many types of copper ore deposits (Barnes and Lightfoot 2005, Hitzman and Valenta 2005, Galley *et al.* 2007, Sillitoe 2010), and its sulfur isotope composition can reveal sulfur source and ore-forming processes (Ohmoto and Goldhaber 1997, Wagner *et al.* 2010, Ulrich *et al.* 2011). However, conventional bulk-mineral isotope analysis produces a combined signature of the desired mineral and unwanted contributions from mineral inclusions, crack impurities, and/or coexisting replacement/exsolution minerals (Chen *et al.* 2010), for example, 'chalcopyrite disease' (exsolution lamellae) in sphalerite (Eldridge *et al.* 1988, Bortnikov *et al.* 1991). Thus, an *in situ* microbeam measurement technique, notably the secondary ion mass spectrometry (SIMS) with high sensitivity and spatial resolution, is required to determine the mineral-specific sulfur isotope ratio (Whitehouse 2013, Ireland *et al.* 2014, Zhang *et al.* 2014a, LaFlamme *et al.* 2016, Zhang *et al.* 2017, Cui *et al.* 2018, Drake *et al.* 2018, Bryant *et al.* 2019). A major issue of SIMS analysis is the instrumental mass fractionation (IMF), which results mainly from the ionisation process (Hartley *et al.* 2012). The IMF caused by the ionisation process is matrix-specific (Valley and Kita 2009, Othmane *et al.* 2015), and currently can only be corrected by analysing reference materials of the same minerals (Othmane *et al.* 2015). However, the well-characterised, high-quality chalcopyrite reference materials for SIMS calibration are scarce (Crowe and Vaughan 1996, Cabral *et al.* 2013, Whitehouse 2013, LaFlamme *et al.* 2016).

doi: 10.1111/ggr.12330

In recent work, CPY-1 ($\delta^{34}S$ = +1.4 ± 0.4‰, 2*s*) (Li *et al.* 2017, 2018), CPY-2 ($\delta^{34}S$ = -0.5 ± 1.0‰, 2*s*) (Molnár *et al.* 2016) and Nifty-b ($\delta^{34}S$ = -3.58 ± 0.44‰, 2*s*) (LaFlamme *et al.* 2016) have been the most widely used working reference material for chalcopyrite sulfur isotope microanalysis, but their quantities are limited and accumulated data have shown some isotopic heterogeneity in CPY-1 and CPY-2 (Molnár *et al.* 2016). In this study, we obtained 607 SIMS and ninety-five LA-MC-ICP-MS sulfur isotope spot measurement results from a natural chalcopyrite sample (HTS4-6) on a cruciform section (plus over 120 randomly selected grains of this chalcopyrite) to assess its potential as a chalcopyrite reference material for *in situ* microbeam sulfur isotope measurements. Our results show that HTS4-6 is sufficiently texturally and chemically homogenous to be used as a reference material, and a total of 102 g of 0.2–1 mm chalcopyrite fragments are available to be shared by LA-MC-ICP-MS or SIMS laboratories world-wide upon request.

Sample description and preparation

The samples used in this study were collected from the Hongtoushan copper–zinc deposit, which has been interpreted to be a volcanogenic massive sulfide (VMS) deposit (Gu *et al.* 2007, Zhang *et al.* 2014b). The Hongtoushan VMS deposit is located in the Archaean Hunbei greenstone belt in Liaoning province (north-eastern China), which consists of the Qingyuan Group gneissic/amphibolitic sequences (Gu *et al.* 2007, Zhang *et al.* 2014b). The Qingyuan Group is divided into the Jinfengling and (overlying) Hongtoushan Formations (Gu *et al.* 2007). The Hongtoushan VMS deposit is located in the upper part of the Hongtoushan Formation, which is composed primarily of interbedded meta-volcanic/sedimentary rocks, including amphibolite, biotite leptynite, biotite gneiss and quartz–feldspar gneiss (Gu *et al.* 2007, Zhu *et al.* 2015). The Hongtoushan deposit is the largest of the eight discovered Archaean VMS Cu–Zn deposits in the area (Gu *et al.* 2007). The host rocks were metamorphosed to upper amphibolite facies, at probably 600–650 °C and 0.8–1.6 GPa (Gu *et al.* 2007, Zhang *et al.* 2014b). Multiphase metamorphism and deformation has greatly modified the distribution patterns and textures of the massive sulfide ores (Zhang *et al.* 2014b). Sample HTS4-6 was collected from the alteration zone of the deposit.

Sample HTS4-6 (Figure 1a) was first split into two halves (Figure 1b); then, cruciform chalcopyrite strips were cut from the profile without any petrographic selection in order to investigate potential systematic sulfur isotope variation at the scale of the whole sample. The chalcopyrite strips were cut into ten shorter ones and cast into three epoxy mounts (Figure 1c). The remaining sample was further crushed (300–1000 μm), and then, ~ 120 chalcopyrite grains were randomly selected and cast into another epoxy mount (Figure 1d). The samples were mounted in the middle of their respective mounts. The epoxy mounts were carefully polished several times with gradually finer diamond paste (from 15 to 1 μm). The mounts were washed first in ethanol and then in de-ionised water, and subsequently placed in an oven and heated at 40 °C for 3 h. The sample mounts were then gold-coated (~ 30 nm thick) before the SIMS analysis.

Sample HTS4-6 is massive and coarse-grained, and comprises mostly chalcopyrite, plus minor quartz and trace amount of other sulfide minerals such as pyrrhotite, pyrite and sphalerite (Figures 1b, d). Rounded or ellipsoidal quartz

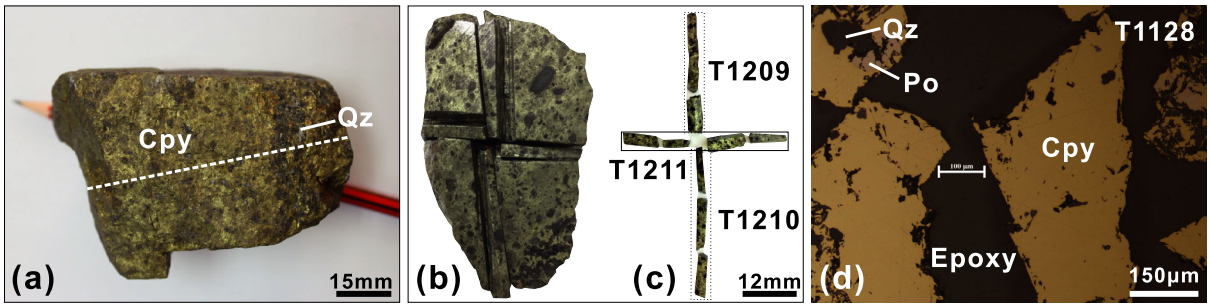

Figure 1. (a) Photograph of HTS4-6 chalcopyrite hand specimen, and the dashed line denotes the location of cruciform chalcopyrite in panel b; (b, c) Photograph of sample HTS4-6 split into two halves, from which chalcopyrite strips were separated and mounted into T1209, T1210 and T1211; (d) sample HTS4-6 chalcopyrite crushed into fine grains and cast into epoxy mount T1128 (reflected light). Abbreviations: Po: pyrrhotite, Cpy: chalcopyrite, Qz: quartz. [Colour figure can be viewed at wileyonlinelibrary.com]

Table 1.
EPMA measurement results for major elements (g/100 g) in HTS4-6 chalcopyrite

Spot ID	Zn	Fe	Cu	Co	S	Total
HTS4-6 Cpy@1	0.06	32.42	33.36	0.05	34.88	100.76
HTS4-6 Cpy@2	0.06	32.17	33.31	0.05	34.86	100.45
HTS4-6 Cpy@3	0.02	32.47	33.28	0.05	35.01	100.82
HTS4-6 Cpy@4	0.02	32.33	33.43	0.05	35.03	100.86
HTS4-6 Cpy@5	0.08	32.33	33.76	0.04	34.78	100.99
HTS4-6 Cpy@6	0.03	32.40	33.82	0.04	34.78	101.07
HTS4-6 Cpy@7	0.02	32.51	33.56	0.05	34.58	100.72
HTS4-6 Cpy@8	0.06	32.38	33.59	0.05	34.59	100.66
HTS4-6 Cpy@9	0.05	32.41	33.30	0.04	34.62	100.41
HTS4-6 Cpy@10	0.04	32.31	33.59	0.04	34.52	100.50
HTS4-6 Cpy@11	0.05	32.23	33.75	0.04	34.46	100.53
HTS4-6 Cpy@12	0.04	32.28	33.30	0.05	34.45	100.12
HTS4-6 Cpy@13	0.06	32.31	33.27	0.05	34.40	100.08
HTS4-6 Cpy@14	0.03	32.37	33.20	0.05	34.27	99.91
HTS4-6 Cpy@15	0.03	32.48	33.75	0.05	34.66	100.96
HTS4-6 Cpy@16	0.05	32.42	33.97	0.04	34.66	101.15
HTS4-6 Cpy@17	0.05	32.66	33.42	0.04	34.66	100.83
HTS4-6 Cpy@18	0.04	32.37	33.51	0.05	34.49	100.46
HTS4-6 Cpy@19	0.04	32.52	33.76	0.05	34.67	101.03
HTS4-6 Cpy@20	0.03	32.46	33.44	0.05	34.55	100.54
HTS4-6 Cpy@21	0.03	32.59	33.41	0.05	34.80	100.87
HTS4-6 Cpy@22	0.03	32.52	33.25	0.05	34.69	100.54
HTS4-6 Cpy@23	0.07	32.39	33.48	0.06	34.30	100.29
HTS4-6 Cpy@24	0.04	32.51	33.46	0.04	34.35	100.40
HTS4-6 Cpy@25	0.04	32.44	33.40	0.05	34.44	100.37
HTS4-6 Cpy@26	0.05	32.43	33.71	0.04	34.55	100.79
HTS4-6 Cpy@27	0.01	32.28	33.42	0.05	34.50	100.27
HTS4-6 Cpy@28	0.01	32.45	33.59	0.05	34.67	100.76
HTS4-6 Cpy@29	0.02	32.56	33.45	0.04	34.48	100.54
HTS4-6 Cpy@30	0.03	32.36	33.80	0.05	34.50	100.74
HTS4-6 Cpy@31	0.04	32.50	33.69	0.06	34.18	100.46
HTS4-6 Cpy@32	0.05	32.26	33.42	0.05	34.46	100.23
HTS4-6 Cpy@33	0.03	32.50	33.62	0.05	34.51	100.71
HTS4-6 Cpy@34	0.03	32.60	33.45	0.05	34.43	100.56
HTS4-6 Cpy@35	0.03	32.35	33.79	0.06	34.30	100.52
HTS4-6 Cpy@36	0.04	32.58	33.57	0.05	34.16	100.39
HTS4-6 Cpy@37	0.04	32.50	33.28	0.06	34.58	100.45
HTS4-6 Cpy@38	0.02	32.22	33.32	0.04	34.42	100.03
HTS4-6 Cpy@39	0.01	32.41	33.58	0.05	34.36	100.41
HTS4-6 Cpy@40	0.03	32.45	33.67	0.04	34.25	100.43
HTS4-6 Cpy@41	0.08	32.56	33.67	0.05	34.40	100.74
HTS4-6 Cpy@42	0.04	32.25	33.54	0.04	34.25	100.11
HTS4-6 Cpy@43	0.03	32.31	33.31	0.06	34.34	100.05
HTS4-6 Cpy@44	0.04	32.48	33.70	0.05	34.41	100.67
HTS4-6 Cpy@45	0.03	32.51	33.73	0.04	34.52	100.83
HTS4-6 Cpy@46	0.05	32.52	33.58	0.05	34.57	100.78
HTS4-6 Cpy@47	0.06	32.44	33.48	0.05	34.32	100.34
HTS4-6 Cpy@48	0.07	32.43	33.28	0.05	34.68	100.52
HTS4-6 Cpy@49	0.05	32.50	33.52	0.04	34.47	100.58
HTS4-6 Cpy@50	0.03	32.57	33.27	0.05	34.35	100.28
HTS4-6 Cpy@51	0.06	32.53	33.77	0.05	35.08	101.51
HTS4-6 Cpy@52	0.07	32.11	33.38	0.05	34.43	100.03
HTS4-6 Cpy@53	0.04	32.47	33.75	0.05	34.33	100.64
HTS4-6 Cpy@54	0.07	32.41	33.40	0.06	34.38	100.32
HTS4-6 Cpy@55	0.05	32.42	33.42	0.06	34.53	100.48
HTS4-6 Cpy@56	0.05	32.40	33.68	0.05	34.57	100.74
HTS4-6 Cpy@57	0.04	32.41	33.48	0.05	34.54	100.52
HTS4-6 Cpy@58	0.03	32.36	33.86	0.06	34.37	100.68
HTS4-6 Cpy@59	0.03	32.45	33.21	0.05	34.47	100.20
HTS4-6 Cpy@60	0.05	32.37	33.56	0.04	34.37	100.40
Mean	0.04	32.42	33.52	0.05	34.52	100.55

Table 1 (continued).
EPMA measurement results for major elements (g/100 g) in HTS4-6 chalcopyrite

Spot ID	Zn	Fe	Cu	Co	S	Total
2*s*	0.03	0.22	0.38	0.01	0.40	0.61

clusters are common, with sizes in the range 1–6 mm, which are distributed randomly throughout the whole sample but are richer in some areas; these are possibly formed from high temperature metamorphic fluid (Zhang *et al.* 2014b). No sign of growth rims on, or any zoning within, the chalcopyrite grains was observed. Quantitative composition analysis using an electron probe microanalyser (EPMA) on the HTS4-6 chalcopyrite (n = 60) showed that the sample is composed of 34.52 ± 0.40 g/100 g S, 33.52 ± 0.38 g/100 g Cu, 32.42 ± 0.22 g/100 g Fe, 0.05 ± 0.01 g/100 g Co, and 0.04 ± 0.03 g/100 g Zn (Table 1). Mineral phases other than chalcopyrite, if present, can be readily avoided by microscopic examination before SIMS analysis.

Analytical techniques

Secondary ion mass spectrometry (SIMS)

The analysis was conducted at the Guangzhou Institute of Geochemistry, Chinese Academy of Sciences (GIGCAS) with a CAMECA IMS 1280-HR instrument. Analytical parameters were similar to those described in Li *et al.* (2019), and are briefly summarised here. A primary $^{133}Cs^{+}$ ion beam (1.5–5.0 nA current and 20 keV total impact energy) was focused on the sample surface. To investigate the potential influence of spot size, three different rasters (i.e., 15, 20 and 30 μm^2) were applied in this study. A 20 s pre-sputtering was undertaken to remove the Au coating, and a normal-incidence electron gun was used for charge compensation. An NMR field sensor was applied to stabilise the magnetic field. ^{32}S, ^{33}S and ^{34}S were measured simultaneously using three Faraday cups (L'2, L1 and H1, respectively). The mass resolving power was set at ~ 5000 to avoid isobaric interference of $^{1}H^{32}S$ to ^{33}S in measurement sessions 1 and 4, and at ~ 2200 (10% height) in sessions 2 and 3 to obtain wide, flat peak tops of the mass spectrum for $^{32}S^{-}$ and $^{34}S^{-}$ ions. The amplifier gains were automatically calibrated before the whole session started. Total analysis time for each spot was ~ 3.5 min. The calibration reference materials used for IMF correction were UWPy-1 (Ushikubo *et al.* 2014), Po-10, PPP-1 (Gilbert *et al.* 2014) and CPY-1 (an in house reference material) for pyrrhotite, pyrite and chalcopyrite, respectively. Data reduction was the same as that described in Li *et al.* (2019), and is briefly summarised below.

Instrumental bias correction factors for $\delta^{3x}S$ were determined by $\delta^{3x}S_{raw}$ of the reference materials (RM) as follows:

$$\alpha_{(SIMS)} = \left(^{3x}S/^{32}S\right)_{RMraw} / \left(^{3x}S/^{32}S\right)_{RMrecommend} \quad (1)$$

$$\left(^{3x}S/^{32}S\right)_{sample} = \left(^{3x}S/^{32}S\right)_{measured} / \alpha_{(SIMS)} \quad (2)$$

where x = 3, 4.

Corrected $^{3x}S/^{32}S$ ratios were normalised to the Vienna Canyon Diablo Troilite (V-CDT) ($^{34}S/^{32}S$ = 1/22.6436, $^{33}S/^{32}S$ = 1/126.948) (Ding *et al.* 2001), according to Equation (3) and taken as the true δ-value ($\delta^{3x}S$).

$$\delta^{3x}S_{sample} = \left[\left(^{3x}S/^{32}S\right)_{sample} / \left(^{3x}S/^{32}S\right)_{V-CDT}\right] - 1 \quad (3)$$

To evaluate the instrumental capability, PPP-1 (Gilbert *et al.* 2014) and UWPy-1 (Ushikubo *et al.* 2014) were also analysed.

Laser ablation MC-ICP-MS

The analysis was conducted with a Nu Plasma 1700 MC-ICP-MS (Nu instruments, UK) at the State Key Laboratory of Continental Dynamics, Northwest University (Xi'an, China). A 193-nm ArF excimer laser ablation system (RESOlution M-50-LR, asi) was used as the ablation source. Argon and ultra-high He were used as auxiliary and carrier gas, and their flow rate was set at 800 and 280 ml min^{-1}, respectively. All measurements were in spot mode with a spot size of 30 μm, 3 Hz repetition rate and 3.6 J cm^{-2} laser energy. Each measurement lasted for 170 s, including a 30 s pre-ablation background measurement, 50 s data acquisition and 90 s washout. Cup configurations for sulfur were H5 and L4 for m/z 34 and 32, respectively. Mass resolution was set at 18000 to avoid isobaric interference. Instrumental drift and mass bias were corrected using the calibrator-sample bracketing technique, with repeated measurement of reference materials before and after every two unknown samples. The reference materials used for data correction were Cpy-1 ($\delta^{34}S$ = +4.2 ± 0.3‰) and NBS123 ($\delta^{34}S$ = +17.8 ± 0.2‰) for chalcopyrite and sphalerite, respectively (Chen *et al.* 2017). More details can be found in Chen *et al.* (2019).

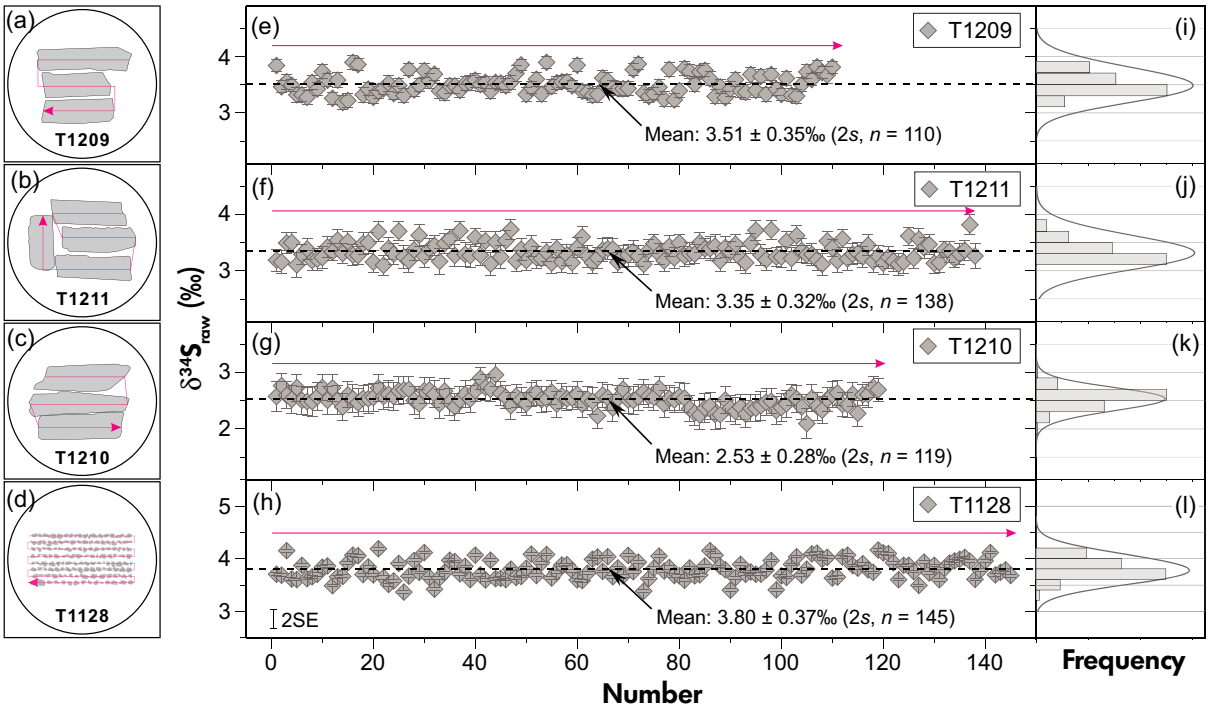

Figure 2. (a)–(d) Sketch maps of the chalcopyrite strips (epoxy mount diameter: 25 mm). Red arrows denote analytical directions. (e)–(h) Raw $\delta^{34}S$ value of HTS4-6 chalcopyrite on mount T1209, T1211, T1210 and T1128. The precisions shown are measurement repeatability only. (i)–(l) Frequency histogram and probability density curves of raw $\delta^{34}S$ values of HTS4-6 chalcopyrite on mounts T1209, T1211, T1210 and T1128. For the probability density plots, the 'external uncertainty' determined by repeated measurement of pyrite reference materials (ranging from 0.17 to 0.48‰, 2*s*) in individual sessions was propagated to the unknowns. [Colour figure can be viewed at wile yonlinelibrary.com]

Gas source isotope ratio mass spectrometry (GS-IRMS)

Sulfur isotope compositions (^{32}S and ^{34}S) of HTS4-6 chalcopyrite were determined by GS-IRMS at both the Beijing Research Institute of Uranium Geology and Institute of Geochemistry, Chinese Academy of Sciences. Grains of chalcopyrite from HTS4-6 were hand picked under a binocular microscope to ensure high purity. The grains were mixed with copper(I) oxide and crushed to 200 mesh. The chalcopyrite was reacted with copper(I) oxide at 980 °C under a vacuum pressure of 2×10^{-2} Pa, and the product SO_2 was measured with a MAT-251 mass spectrometer. The measurement precision, expressed as twice the standard deviation, was better than ± 0.2‰.

Quadruple sulfur isotope composition (^{32}S, ^{33}S, ^{34}S and ^{36}S) of HTS4-6 was also determined by GS-IRMS at the University of Maryland, College Park (UMCP). The measurement procedure was as in Wu *et al.* (2018) and is briefly summarised here. Sulfur in the chalcopyrite was extracted

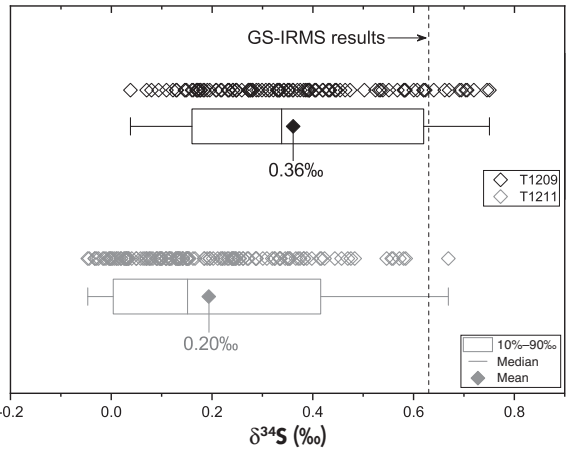

Figure 3. IMF-corrected $\delta^{34}S$ values for HTS4-6 chalcopyrite analysed in session 1. The repeatability precision of individual spots is 0.10 to 0.20‰ (2SE).

with a 5 mol l^{-1} HCl (10 ml) + acidic 0.3 mol l^{-1} Cr (II) (20 ml) solution, and the produced hydrogen sulfide was trapped as zinc sulfide, which was subsequently fluorinated

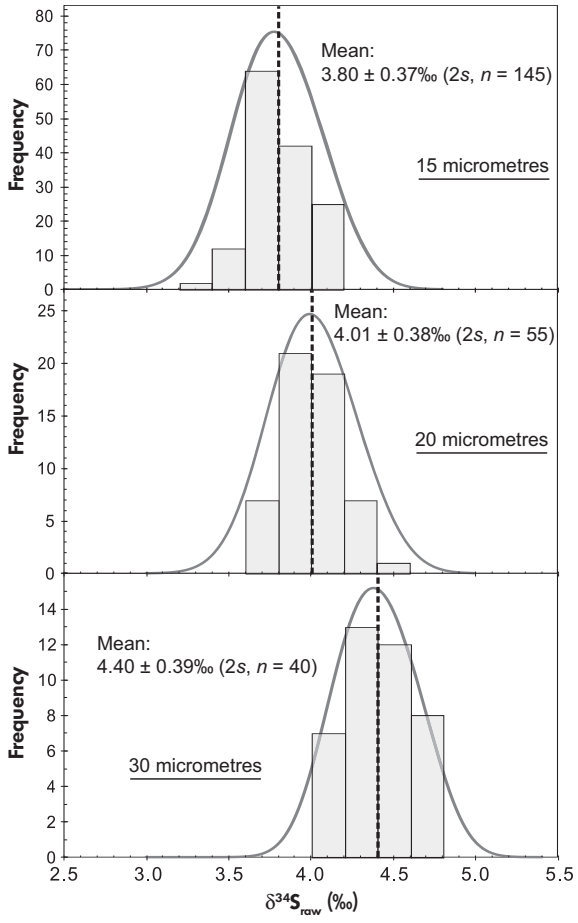

Figure 4. Comparison of raw $\delta^{34}S$ values of HTS4-6 chalcopyrite with various spot sizes (15, 20, 30 μm). For the probability density plots, the 'external uncertainty' determined by repeated measurement of pyrite reference materials (ranging from 0.17 to 0.48‰, 2s) in individual sessions was propagated to the unknowns.

to produce sulfur hexafluoride (SF_6). After that, the SF_6 gas was collected via freezing with liquid nitrogen and then analysed for quadruple sulfur isotopes using a dual-inlet Thermo-Finnigan MAT 253 GS-IRMS. The data were normalised to V-CDT and reported in per mil (parts per thousand, ‰) using the $\delta^{34}S$, $\Delta^{33}S$, and $\Delta^{36}S$ notation, where $\delta^{3x}S = ({}^{3x}S/{}^{32}S)_{sample}/({}^{3x}S/{}^{32}S)_{reference} - 1$ (x = 3, 4, 6); $\Delta^{33}S = \delta^{33}S - ((1 + \delta^{34}S)^{0.515} - 1)$; and $\Delta^{36}S = \delta^{36}S - ((1 + \delta^{34}S)^{1.90} - 1)$. The intermediate precision of the measurement results of HTS4-6 is the intermediate precision results obtained on isotope RM IAEA-S1 (Ag_2S) over a longer time period, which yielded $\delta^{34}S$ = -0.30 ± 0.03‰, $\Delta^{33}S$ = +0.09 ± 0.01‰ and $\Delta^{36}S$ = -0.69 ± 0.03‰ (2*s*, *n* = 5).

Electron probe microanalysis

The major element mass fractions of HTS4-6 were determined using a JEOL JXA-8230 electron probe microanalyser at the same laboratory as the SIMS analysis. Analytical conditions for all elements include 20 kV accelerating voltage, 20 nA beam current and 1 μm beam size.

Results

EPMA data are listed in Table 1. Results from four separate SIMS measurement sessions for HTS4-6 are displayed in Figures 2, 3 and 4. SIMS sulfur isotope compositions of PPP-1 corrected by UWPy-1 are listed in Table 2. The LA-MC-ICP-MS and GS-IRMS results are displayed in Figures 5 and 6. More details are given in online supporting information Tables S1 and S2.

SIMS measurement results

The spot measurements were performed continuously on the chalcopyrite strips with steps of 300–500 μm (Figure 2a–c). For each randomly selected grain, measurements were undertaken on one to two spots (Figure 2d). The mean raw $\delta^{34}S$ values for HTS4-6 on grains from the two mounts measured in session 1 were +3.51 ± 0.35‰ (2*s*, *n* = 110, T1209) and +3.35 ± 0.32‰ (2*s*, *n* = 138, T1211), respectively (Figure 2e, f), whilst those in session 2 and 3 are +2.53 ± 0.28‰ (2*s*, *n* = 119, T1210) and +3.80 ± 0.37‰ (2*s*, *n* = 145, T1128), respectively (Figure 2g, h). Most of the results (from all four mounts) show normal distributions in the probability density plots (Figure 2i–l), and the slightly skew pattern in Figure 2i may be resulted from the sample-topography effect (Kita *et al.* 2009) led by the hardness difference between quartz and chalcopyrite.

In session 1, the chalcopyrite strips (data corrected by the in house reference material CPY-1) yielded mean $\delta^{34}S$ values of +0.36 ± 0.35‰ (T1209; 2*s*, *n* = 110) and +0.20 ± 0.32‰ (T1211; 2*s*, *n* = 138) (Figure 3). The reference material CPY-1 yielded a mean $\delta^{34}S$ = +1.4 ± 0.93‰ (2*s*, *n* = 15) (Table S1), and a between-spot intermediate measurement precision of 0.93‰, showing that this sample is not highly homogeneous. The $\delta^{34}S$ values of HTS4-6 (CPY-1 corrected) are systematically lower than those obtained by GS-IRMS, also indicating the heterogeneity of CPY-1. Thus, the CPY-1 chalcopyrite was not used for IMF corrections in the subsequent sessions, and only raw (i.e., not IMF-corrected) values are reported from those later sessions.

Table 2.
SIMS sulfur isotope composition of PPP-1 corrected by UWPy-1 (‰)

Sample ID	Current (nA)	^{32}S/Coeff L′2		$^{33}S/^{32}S$ L1/L′2	SE (%)	$^{34}S/^{32}S$ H1/L′2	SE (%)	$\delta^{33}S$ (‰)	2*s* (‰)	$\delta^{34}S$ (‰)	2*s* (‰)	$\Delta^{33}S$ (‰)	2*s* (‰)
T191 PPP-1 15 Micron@01	2.8	1.47E+09	0.04	0.0079	0.008	0.0445	0.003	2.68	0.24	5.39	0.44	-0.10	0.06
T191 PPP-1 15 Micron@02	2.8	1.47E+09	0.02	0.0079	0.008	0.0446	0.003	2.85	0.24	5.51	0.44	0.02	0.06
T191 PPP-1 15 Micron@03	2.8	1.48E+09	0.01	0.0079	0.008	0.0445	0.003	2.57	0.24	5.24	0.44	-0.13	0.06
T191 PPP-1 15 Micron@04	2.8	1.49E+09	0.03	0.0079	0.008	0.0445	0.003	2.68	0.24	5.32	0.44	-0.06	0.06
T191 PPP-1 15 Micron@05	2.8	1.49E+09	0.02	0.0079	0.008	0.0445	0.003	2.73	0.24	5.30	0.44	0.00	0.06
T191 PPP-1 15 Micron@06	2.8	1.33E+09	0.03	0.0079	0.009	0.0446	0.004	2.56	0.24	5.47	0.44	-0.26	0.06
T191 PPP-1 15 Micron@07	2.8	1.33E+09	0.02	0.0079	0.009	0.0446	0.004	2.60	0.24	5.46	0.44	-0.21	0.06
T191 PPP-1 15 Micron@08	2.8	1.37E+09	0.02	0.0079	0.009	0.0446	0.004	2.81	0.24	5.64	0.44	-0.09	0.06
T191 PPP-1 15 Micron@09	2.8	1.33E+09	0.02	0.0079	0.009	0.0446	0.004	2.83	0.24	5.60	0.44	-0.05	0.06
T191 PPP-1 15 Micron@10	2.8	1.35E+09	0.02	0.0079	0.009	0.0446	0.004	2.82	0.24	5.50	0.44	-0.01	0.06
Mean								2.71		5.45		-0.09	
2*s*								0.23		0.26		0.18	
T191 UWPy-1 15 Micron@01	2.9	1.65E+09	0.02	0.0080	0.008	0.0450	0.003	8.36	0.24	16.24	0.44	0.03	0.06
T191 UWPy-1 15 Micron@02	2.9	1.63E+09	0.06	0.0080	0.008	0.0450	0.003	8.17	0.24	16.00	0.44	-0.04	0.06
T191 UWPy-1 15 Micron@03	2.9	1.61E+09	0.05	0.0080	0.008	0.0450	0.003	8.26	0.24	16.03	0.44	0.04	0.06
T191 UWPy-1 15 Micron@04	2.9	1.66E+09	0.02	0.0080	0.008	0.0450	0.003	8.25	0.24	16.09	0.44	0.00	0.06
T191 UWPy-1 15 Micron@05	2.9	1.63E+09	0.08	0.0080	0.008	0.0450	0.003	8.36	0.24	16.25	0.44	0.02	0.06
T191 UWPy-1 15 Micron@06	2.9	1.63E+09	0.02	0.0080	0.008	0.0450	0.003	8.35	0.24	16.26	0.44	0.01	0.06
T191 UWPy-1 15 Micron@07	2.9	1.62E+09	0.03	0.0080	0.008	0.0450	0.003	8.22	0.24	16.11	0.44	-0.04	0.06
T191 UWPy-1 15 Micron@08	2.9	1.59E+09	0.03	0.0080	0.008	0.0450	0.003	8.09	0.24	15.81	0.44	-0.02	0.06
T191 UWPy-1 15 Micron@09	2.9	1.58E+09	0.08	0.0080	0.008	0.0450	0.004	8.00	0.24	15.54	0.44	0.02	0.06
T191 UWPy-1 15 Micron@10	2.9	1.62E+09	0.01	0.0080	0.008	0.0450	0.003	8.25	0.24	16.08	0.44	0.00	0.06
Mean								8.23		16.04		0.00	
2*s*								0.24		0.44		0.06	
T749 PPP-1 20 micron@1	3.2	1.81E+09	0.04	0.0079	0.007	0.0446	0.003	3.21	0.11	5.98	0.38	0.13	0.12
T749 PPP-1 20 micron@2	3.2	1.79E+09	0.04	0.0079	0.008	0.0446	0.003	2.97	0.11	5.96	0.38	-0.09	0.12
T749 PPP-1 20 micron@3	3.2	1.81E+09	0.04	0.0079	0.007	0.0446	0.003	2.90	0.11	5.72	0.38	-0.05	0.12
T749 PPP-1 20 micron@4	3.2	1.82E+09	0.03	0.0079	0.007	0.0446	0.003	3.06	0.11	5.87	0.38	0.04	0.12
T749 PPP-1 20 micron@5	3.2	1.79E+09	0.03	0.0079	0.008	0.0446	0.003	2.90	0.11	5.72	0.38	-0.04	0.12
T749 PPP-1 20 micron@6	3.2	1.81E+09	0.03	0.0079	0.007	0.0446	0.003	2.95	0.11	5.83	0.38	-0.04	0.12
Mean								3.00		5.85		-0.01	
2*s*								0.24		0.22		0.16	
T749 UWPy-1 20 micron@1	3.1	1.75E+09	0.05	0.0080	0.008	0.0450	0.003	8.18	0.11	16.07	0.38	-0.06	0.24
T749 UWPy-1 20 micron@2	3.1	1.73E+09	0.02	0.0080	0.008	0.0450	0.003	8.15	0.11	15.96	0.38	-0.03	0.24
T749 UWPy-1 20 micron@3	3.1	1.74E+09	0.03	0.0080	0.008	0.0450	0.003	8.22	0.11	16.11	0.38	-0.04	0.24
T749 UWPy-1 20 micron@4	3.1	1.72E+09	0.06	0.0080	0.008	0.0450	0.003	8.27	0.11	16.03	0.38	0.05	0.24

GEOSTANDARDS and GEOANALYTICAL RESEARCH

Table 2 (continued).
SIMS sulfur isotope composition of PPP-1 corrected by UWPy-1 (‰)

Sample ID	Current (nA)	^{32}S/Coeff L'2		$^{33}S/^{32}S$ L1/L'2	SE (%)	$^{34}S/^{32}S$ H1/L'2	SE (%)	$\delta^{33}S$ (‰)	2s (‰)	$\delta^{34}S$ (‰)	2s (‰)	$\Delta^{33}S$ (‰)	2s (‰)
T749 UWPy-1 20 micron@5	3.1	1.73E+09	0.04	0.0080	0.008	0.0450	0.003	8.30	0.11	15.75	0.38	0.22	0.24
T749 UWPy-1 20 micron@6	3.1	1.80E+09	0.12	0.0080	0.007	0.0450	0.003	8.25	0.11	16.33	0.38	-0.13	0.24
Mean								8.23		16.04		0.00	
2s								0.11		0.13		0.12	
T749 PPP-1 30 Micron@1	5.0	2.95E+09	0.05	0.0079	0.006	0.0446	0.002	3.06	0.18	6.03	0.31	-0.04	0.09
T749 PPP-1 30 Micron@2	5.0	2.98E+09	0.03	0.0079	0.006	0.0446	0.002	2.99	0.18	5.87	0.31	-0.03	0.09
T749 PPP-1 30 Micron@3	5.0	2.98E+09	0.04	0.0079	0.006	0.0446	0.002	2.96	0.18	5.87	0.31	-0.06	0.09
T749 PPP-1 30 Micron@4	5.0	2.95E+09	0.04	0.0079	0.006	0.0446	0.002	2.98	0.18	5.89	0.31	-0.05	0.09
T749 PPP-1 30 Micron@5	5.0	3.05E+09	0.06	0.0079	0.006	0.0446	0.002	2.91	0.18	5.81	0.31	-0.08	0.09
T749 PPP-1 30 Micron@6	5.0	3.01E+09	0.06	0.0079	0.006	0.0446	0.002	3.11	0.18	5.99	0.31	0.03	0.09
Mean								3.00		5.91		-0.04	
2s								0.15		0.17		0.07	
T749 UWPy-1 30 Micron@1	5.0	3.03E+09	0.04	0.0080	0.006	0.0451	0.002	8.32	0.18	16.12	0.31	0.05	0.09
T749 UWPy-1 30 Micron@2	5.0	3.05E+09	0.04	0.0080	0.006	0.0451	0.002	8.22	0.18	16.10	0.31	-0.03	0.09
T749 UWPy-1 30 Micron@3	5.0	3.04E+09	0.03	0.0080	0.006	0.0451	0.002	8.27	0.18	16.22	0.31	-0.05	0.09
T749 UWPy-1 30 Micron@4	5.0	3.03E+09	0.03	0.0080	0.006	0.0451	0.002	8.25	0.18	15.97	0.31	0.06	0.09
T749 UWPy-1 30 Micron@5	5.0	3.02E+09	0.05	0.0080	0.006	0.0451	0.002	8.26	0.18	16.06	0.31	0.02	0.09
T749 UWPy-1 30 Micron@6	5.0	2.96E+09	0.03	0.0080	0.006	0.0450	0.002	8.06	0.18	15.77	0.31	-0.03	0.09
Mean								8.23		16.04		0.00	
2s								0.18		0.31		0.09	

Table 3.
GS-IRMS sulfur isotope results for HTS4-6 chalcopyrite (‰)

Sample ID	$\delta^{33}S$	2*s*	$\delta^{34}S$	2*s*	$\delta^{36}S$	2*s*	$\Delta^{33}S$	2*s*	$\Delta^{36}S$	2*s*
HTS4-6@1 [a]	0.26	0.02	0.62	0.03	1.22	0.04	-0.06	0.01	0.04	0.03
HTS4-6@2 [a]	0.26	0.02	0.62	0.03	1.24	0.04	-0.06	0.01	0.07	0.03
HTS4-6@3 [a]	0.26	0.02	0.62	0.03	1.25	0.04	-0.06	0.01	0.07	0.03
Mean	0.26	0.01	0.62	0.01	1.23	0.03	-0.06	0.01	0.06	0.04
IAEA-S1@1 [a]	-0.08	0.02	-0.28	0.03	-1.25	0.04	0.09	0.01	-0.71	0.03
IAEA-S1@2 [a]	-0.06	0.02	-0.30	0.03	-1.25	0.04	0.10	0.01	-0.67	0.03
IAEA-S1@3 [a]	-0.08	0.02	-0.29	0.03	-1.25	0.04	0.10	0.01	-0.69	0.03
IAEA-S1@4 [a]	-0.08	0.02	-0.33	0.03	-1.30	0.04	0.09	0.01	-0.68	0.03
IAEA-S1@5 [a]	-0.06	0.02	-0.30	0.03	-1.26	0.04	0.09	0.01	-0.69	0.03
Mean [a]	-0.06	0.02	-0.30	0.03	-1.26	0.04	0.09	0.01	-0.69	0.03
HTS4-6@1 [b]			0.54	0.20						
HTS4-6@2 [b]			0.65	0.20						
HTS4-6@3 [b]			0.65	0.20						
HTS4-6@4 [b]			0.62	0.20						
HTS4-6@5 [b]			0.68	0.20						
HTS4-6@6 [b]			0.62	0.20						
HTS4-6@7 [b]			0.68	0.20						
HTS4-6@8 [b]			0.69	0.20						
HTS4-6@9 [b]			0.70	0.20						
HTS4-6@10 [b]			0.55	0.20						
Mean [b]			0.64	0.11						
HTS-4-6-1 [c]			0.60	0.20						
HTS-4-6-2 [c]			0.60	0.20						
HTS-4-6-3 [c]			0.70	0.20						
HTS-4-6-4 [c]			0.60	0.20						
HTS-4-6-5 [c]			0.70	0.20						
HTS-4-6-6 [c]			0.80	0.20						
HTS-4-6-7 [c]			0.40	0.20						
HTS-4-6-8 [c]			0.60	0.20						
HTS-4-6-9 [c]			0.50	0.20						
HTS-4-6-10 [c]			0.70	0.20						
Mean [c]			0.62	0.23						

Sample ID with '[a]', '[b]' and '[c]' were analysed at University of Maryland, Institute of Geochemistry and Beijing Research Institute of Uranium Geology, respectively.

Spot sizes of 20 and 30 μm were used in session 4, and the analyses were made on grains on the same mount also analysed in session 3 (T1128). The results obtained in session 4 are compared with those from session 3 (Figure 4). The results show that the repeatability precision of raw $\delta^{34}S$ value with spot sizes of 15, 20 and 30 μm were 0.37, 0.38 and 0.39‰, respectively. No obvious change in the precision of raw $\delta^{34}S$ values was observed when different spot sizes were used (Figure 4).

Two mounts (T191 and T749) with both PPP-1 and UWPy-1 were analysed to evaluate the instrumental capability. The PPP-1 on T749 analysed with two different spot sizes (20 and 30 μm) yielded similar mean $\delta^{34}S$ values at +5.85 ± 0.22‰ (2*s*, *n* = 6) and +5.91 ± 0.17‰ (2*s*, *n* = 6) (Table 2). The PPP-1 on T191 analysed with 15 μm spot size yielded a mean value of +5.45 ± 0.26‰ (2*s*, *n* = 10). The corrected $\delta^{34}S$ values for PPP-1 on T749 are ~0.5‰ higher than the recommended value (+5.3 ± 0.2‰, Gilbert *et al.* 2014), but that on T191 is similar to the recommended value. The broad consistency of the corrected value for PPP-1 indicates the instrumental capability of our laboratory, and the mildly higher $\delta^{34}S$ value on T749 may reflect the slight $\delta^{34}S$ heterogeneity in PPP-1.

LA-MC-ICP-MS measurement results

The homogeneity of HTS4-6 chalcopyrite was further evaluated using LA-MC-ICP-MS. A total of ninety-six spot analyses on the HTS4-6 chalcopyrite were conducted, which yielded a normal distribution of $\delta^{34}S$ values, with a mean of +0.58 ± 0.38‰ (2*s*, *n* = 95) (Figure 5).

GS-IRMS measurement results

Randomly selected fragments of the HTS4-6 chalcopyrite were analysed twenty-three times by GS-IRMS, yielding a mean $\delta^{34}S$ = +0.63 ± 0.16‰ (2*s*, *n* = 23). The mean $\delta^{33}S$ and $\delta^{36}S$ were determined to be +0.26 ± 0.01‰ and +1.23 ± 0.03‰ (2*s*, *n* = 3), respectively. Detailed measurement results are given in Table 3 and Figure 6.

Table 4.
Sulfur isotope results for pyrrhotite, pyrite and sphalerite in sample HTS4-6 (‰)

Sample ID	$\delta^{33}S$	2*s*	$\delta^{34}S$	2*s*	$\Delta^{33}S$	2*s*
T1128 HTS4-6 Po@1	-0.34	0.23	-0.07	0.22	-0.30	0.16
T1128 HTS4-6 Po@2	-0.08	0.23	0.35	0.22	-0.26	0.16
T1128 HTS4-6 Po@3	-0.04	0.23	0.34	0.22	-0.21	0.16
T1128 HTS4-6 Po@4	-0.53	0.23	-0.60	0.22	-0.23	0.16
T1128 HTS4-6 Po@5	0.08	0.23	0.41	0.22	-0.13	0.16
T1128 HTS4-6 Po@6	-0.26	0.23	0.00	0.22	-0.26	0.16
T1128 HTS4-6 Po@7	0.03	0.23	0.34	0.22	-0.15	0.16
T1128 HTS4-6 Po@8	0.21	0.23	0.72	0.22	-0.16	0.16
Mean	-0.12		0.18		-0.21	
T1128 HTS4-6 Py@1	0.13	0.24	0.38	0.44	-0.07	0.06
T1128 HTS4-6 Py@2	-0.11	0.24	-0.08	0.44	-0.07	0.06
T1128 HTS4-6 Py@3	0.01	0.24	0.41	0.44	-0.21	0.06
T1128 HTS4-6 Py@4	0.30	0.24	0.65	0.44	-0.03	0.06
Mean	0.06		0.34		-0.10	
Mount HTS4-6 Sph@1			0.97	0.18		
Mount HTS4-6 Sph@2			0.50	0.18		
Mount HTS4-6 Sph@3			0.88	0.18		
Mount HTS4-6 Sph@4			0.62	0.18		
Mount HTS4-6 Sph@5			0.34	0.18		
Mount HTS4-6 Sph@6			0.65	0.18		
Mean			0.66			

Po: pyrrhotite; Py: pyrite; Sph: sphalerite. Pyrrhotite and pyrite were determined using secondary ion mass spectrometry (SIMS), and sphalerite was determined using laser ablation coupled with multi-collector inductively coupled plasma-mass spectrometry (LA-MC-ICP-MS).

$\delta^{34}S$ values of other sulfide minerals (pyrrhotite, pyrite and sphalerite) in sample HTS4-6 have potentially important influence on the GS-IRMS results for chalcopyrite in the sample. Sulfur isotope ratios of pyrrhotite and pyrite were determined by SIMS, and sphalerite by LA-MC-ICP-MS. The mean $\delta^{34}S$ values of pyrrhotite, pyrite and sphalerite in HTS4-6 are +0.18‰ (n = 8), +0.34‰ (n = 4) and +0.66‰ (n = 6) (Table 4), respectively. This indicates that the sulfur of these other sulfide minerals are similar to those of chalcopyrite, and thus, minor contamination from them would only have negligible effect on the GS-IRMS results for the chalcopyrite. This conclusion is supported by the consistent results obtained from LA-MC-ICP-MS and GS-IRMS.

Discussion

Homogeneity of HTS4-6 chalcopyrite

As mentioned previously, two approaches were used to evaluate the sulfur isotopic homogeneity of sample HTS4-6; that is, measurement of cruciform chalcopyrite strips cut from the sample profile (Figure 1c), and randomly selected chalcopyrite grains from the crushed sample (Figure 1d). $\delta^{34}S$ precision of the mean expressed as 2s standard deviation in all the three chalcopyrite strips determined using SIMS ranged from 0.28 to 0.35‰, and no systematic variation was observed (Figures 2e–g), indicating good sulfur isotopic homogeneity of the chalcopyrite strips. The precision of the mean of raw $\delta^{34}S$ values of the randomly selected grains, which is assumed to be representative of the whole sample, was 0.37‰ (2s) (Figure 2h), which is similar to that of the profile analyses results. The data obtained from LA-MC-ICP-MS gave a precision of the mean of 0.38‰ (2s) for $\delta^{34}S$, similar to their SIMS-derived counterparts (Figure 5). These altogether demonstrate that the homogeneity of HTS4-6 is comparable to UWPy-1 and PPP-1.

SIMS measurement results from different spot sizes (15, 20 and 30 μm) on the grains from mount T1128 were evaluated to investigate its potential influence on measurement precision. This showed no evident correlation between spot size and the intermediate precision, except that larger spot sizes with higher beam current would result in higher raw $\delta^{34}S$ values (Figure 4).

Table 5.
Summary table with the key values from all measurement sessions in this study

Session	Sample ID	Weighted mean $\delta^{34}S$ (‰)	2*s* (‰)	Median spot 2SE (‰)	MSWD	Excess error (2σ) (‰)	Number	Number of rejections
1	T1209	3.51 [a]	0.35	0.12	9.2	0.33	110	0
1	T1211	3.34 [a]	0.32	0.19	3.2	0.27	138	0
1	UWPy-1	19.22 [a]	0.48	0.12	8.5	0.41	20	1
2	T1210	2.53 [a]	0.28	0.23	1.5	0.17	119	0
2	UWPy-1	19.05 [a]	0.22	0.18	1.3	0.00	15	3
3	T1128	3.80 [a]	0.37	0.03	196.0	0.37	145	0
3	PPP-1	9.21 [a]	0.39	0.03	175.0	0.38	30	0
4	T1128 (20 μm)	4.01 [a]	0.38	0.07	32.0	0.37	55	0
4	T1128 (30 μm)	4.40 [a]	0.39	0.05	58.0	0.38	40	0
4	T191 PPP-1 (15 μm)	8.77 [a]	0.26	0.07	13.0	0.23	10	0
4	T191 UWPy-1 (15 μm)	19.37 [a]	0.24	0.07	33.0	0.41	10	0
4	T749 PPP-1 (20 μm)	9.55 [a]	0.22	0.06	13.0	0.19	6	0
4	T749 UWPy-1 (20 μm)	19.74 [a]	0.38	0.06	37.0	0.34	6	0
4	T749 PPP-1 (30 μm)	10.05 [a]	0.17	0.05	12.0	0.15	6	0
4	T749 UWPy-1 (30 μm)	20.18 [a]	0.31	0.05	41.0	0.28	6	0
	T1128 (LA-MC-ICP-MS)	0.58 [b]	0.38	0.13	8.2	0.35	95	0

Number with '[a]' and '[b]' is raw and IMF-corrected $\delta^{34}S$ values, respectively. Excess error was calculated using Isoplot.

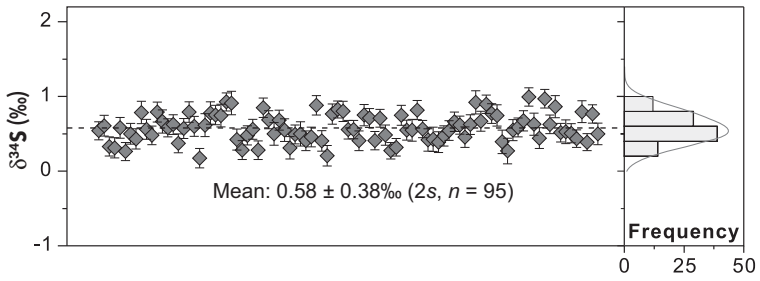

Figure 5. $\delta^{34}S$ values of HTS4-6 chalcopyrite determined by LA-MC-ICP-MS. For the probability density plots, the 'external uncertainty' determined by repeated measurement of pyrite reference materials (ranging from 0.17 to 0.48‰, 2*s*) in individual sessions was propagated to the unknowns.

In addition to precision estimates, an *F*-test and homogeneity index (*H*) were also applied to further characterise the sulfur isotopic homogeneity of HTS4-6. Following the guidance for characterisation, and assessment of homogeneity and stability (ISO Guide 35 2017), an *F*-test on the sulfur isotope data was applied by comparing HTS4-6 with repeated measurements of the well-characterised reference materials UWPy-1 (multiple grains, session 1, 2 and 4) (Ushikubo *et al.* 2014) and PPP-1 (one grain, session 3) pyrite (Gilbert *et al.* 2014). Results of the *F*-test indicate that the standard deviations of all sessions (strips and grains) of HTS4-6 are equal at the 95% confidence level to the standard deviations of the analyses of UWPy-1 and PPP-1 (Table S1)).

The *H*-index represents the ratio of the measurement precision to the expected total combined uncertainty and includes both instrumental uncertainty and sample heterogeneity (Batanova *et al.* 2019). *H*-index = 1 implies that the sample is homogeneous within the measurement uncertainty of individual measurements, whereas *H*-index > 3 indicates significant isotopic heterogeneity (Batanova *et al.* 2019). Since no proper chalcopyrite reference material was available, pyrite reference material UWPy-1 and PPP-1 were used to constrain the 'measurement uncertainty'. For HTS4-6, the obtained *H*-indices cluster around 1 (max 1.3), indicating good isotopic homogeneity (Figure 7).

The mean square weighted deviation (MSWD) of the repeat measurement results was used to estimate sample homogeneity (Gilbert *et al.* 2014), where a MSWD close to 1 indicates that the variance of repeat measurements can be explained by within-spot uncertainty, which suggests homogeneity of a given sample within analytical uncertainty.

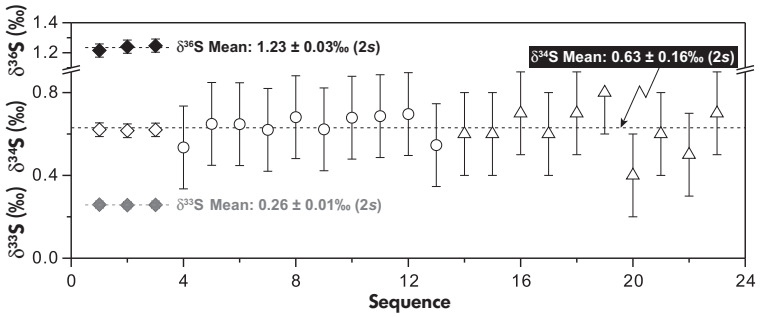

Figure 6. $\delta^{33}S$, $\delta^{34}S$ and $\delta^{36}S$ values of HTS4-6 chalcopyrite determined by GS-IRMS. The rhombuses denote data obtained from University of Maryland, circles from Institute of Geochemistry and triangles from Beijing Research Institute of Uranium Geology.

All data derived from SIMS and LA-MC-ICP-MS measurement sessions were processed using Isoplot, and the results are presented in Table 5. The MSWD of HTS4-6 in all SIMS sessions had a very wide range, typically 1.5 to 196. This range is similar to the pyrite reference materials used in this study. The very high MSWD in session 3 (for both HTS4-6 and PPP-1) results from the small error for individual measurements (2SE). The MSWD of HTS4-6 is greater than 1, suggesting that the variation in HTS4-6 exceeds what is expected from counting statistics alone for all sessions. This can only be explained by the following: (a) the instrument performance having added additional errors on top of the counting errors, which generally happens most of time, as no reference material was used to monitor and correct instrumental drift; (b) there is detectable heterogeneity in HTS4-6. The MSWD and standard derivation of the analytical results for HTS4-6 are similar to or slightly higher than those of UWPy-1 and PPP-1. This is consistent with the fact that both UWPy-1 and PPP-1 have been reported to have some heterogeneity in their sulfur isotope composition

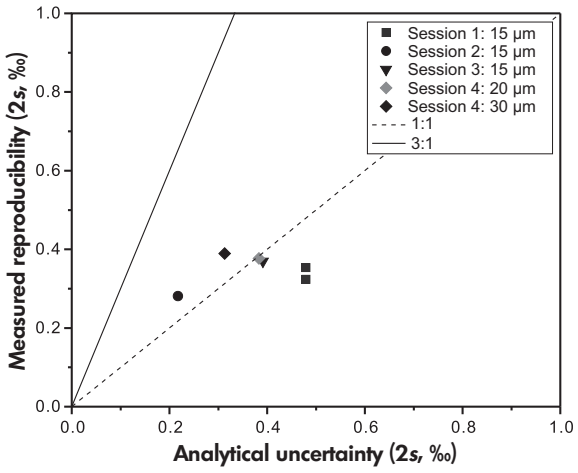

Figure 7. Assessment of homogeneity of sample HTS4-6 chalcopyrite. Values of homogeneity index of 1 (dash-dotted line) and 3 (solid line) are shown.

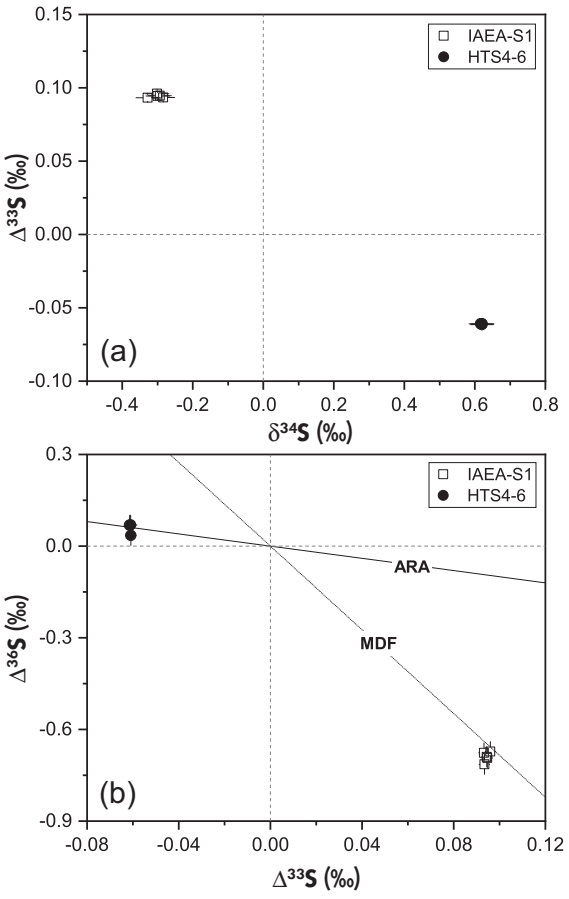

Figure 8. (a) $\delta^{34}S$ vs. $\Delta^{33}S$ diagram and (b) $\Delta^{33}S$ vs. $\Delta^{36}S$ diagram of HTS4-6 determined by GS-IRMS. ARA: Archaean Reference Array; MDF: mass-dependent fractionation.

(Gilbert *et al.* 2014, Ushikubo *et al.* 2014) However, the MSWD for LA-MC-ICP-MS measurement sessions with instrumental drift correction was 8.2, suggesting there is some heterogeneity in HTS4-6 chalcopyrite. An unbiased conclusion would be that the observed $\delta^{34}S$ variability in HTS4-6 is no more than ± 0.40 ‰ (2*s*) at the scale of the whole sample (millimetres).

In sum, the narrow $\delta^{34}S$ range and its normal distribution, the *F*-test results, and the *H*-index demonstrate good isotopic homogeneity of HTS4-6, which is comparable to the well-characterised pyrite reference materials Ruttan and UWPy-1 (Drake *et al.* 2013, Whitehouse 2013, Ushikubo *et al.* 2014) and pyrrhotite YP136 (Li *et al.* 2019).

The mean IMF-corrected SIMS $\delta^{34}S$ values of the grains from two mounts analysed in session 1 (+0.36 ± 0.35‰ (2*s*, *n* = 110) and +0.20 ± 0.32‰ (2*s*, *n* = 138), respectively) are both slightly lower than those determined by GS-IRMS (+0.63 ± 0.16‰, 2*s*, *n* = 23) (Figure 6). However, the LA-MC-ICP-MS results (mean $\delta^{34}S$ = +0.58 ± 0.38‰, 2*s*, *n* = 95) are in good agreement with the GS-IRMS results (mean $\delta^{34}S$ = +0.63 ± 0.16‰, 2*s*, *n* = 23). This indicates that the discrepancy between the IMF-corrected SIMS and GS-IRMS results is probably an artefact resulting from the heterogeneity of the chalcopyrite reference material CPY-1, which gave a much larger between-spot precision (0.93‰, 2*s*) than that of HTS4-6 (Table S1)). Therefore, we suggest that HTS4-6 is a more homogeneous primary reference material in terms of S isotopes than CPY-1 for *in situ* SIMS/LA-MC-ICP-MS sulfur isotope measurement.

The chalcopyrite $\delta^{34}S$ values of HTS4-6 are ~0‰ (Figure 8a), resembling typical mantle-derived sulfur isotopic compositions (Seal 2006), and indicate a largely magmatic sulfur source. This is similar to the chalcopyrite from many other (both ancient and modern) VMS deposits (Ono *et al.* 2007, Chen *et al.* 2015). However, the GS-IRMS results suggest that HTS4-6 has a slightly negative $\Delta^{33}S$ value (Figure 8a). In the $\Delta^{33}S$ vs. $\Delta^{36}S$ diagram, the HTS4-6 data lie on the Archaean Reference Array (ARA) (slope ≈ -1, Figure 7b) (Shen *et al.* 2009, Ono 2017). This indicates that a minor part of the sulfur may have had an atmospheric origin, as has been inferred by other authors (Farquhar *et al.* 2000, 2003, Paris *et al.* 2014).

Mount-to-mount fractionation

The difference of mean raw $\delta^{34}S$ values of HTS4-6 in session 1 is small (0.16‰; Figures 2a-b), which indicates that when the analytical parameters are kept constant, the IMF of chalcopyrite should remain stable during the mount changing process. This demonstrates the reliability of the off-mount calibration procedure for chalcopyrite and agrees with our previous findings for pyrite and pyrrhotite (Li *et al.* 2019).

Conclusions

The measurement precision of HTS4-6 chalcopyrite from both SIMS and LA-MC-ICP-MS analyses was better than 0.39‰ ($^{34}S/^{32}S$, 2*s*). This, together with *F*-test and *H*-index results, indicates comparability to the well-characterised pyrite reference materials Ruttan and UWPy-1, and pyrrhotite YP136. The observed $\delta^{34}S$ variability in HTS4-6 is no more than ± 0.40‰ (2*s*) at the scale of the whole sample and thus a potential reference material for *in situ* microbeam isotopic measurements. We propose a recommended $\delta^{34}S$ value (determined by GS-IRMS) of +0.63 ± 0.16‰ (2*s*, *n* = 23) for the HTS4-6 chalcopyrite.

Acknowledgements

We thank Dr. Mingtian Zhu for his generous sample donation and Dr. Yanyan Zhou for the sample shipping. Profs. Honglin Yuan, Mang Lin and Yanan Shen, and Drs. Kaiyun Chen, Jing Gu and Juan Han are thanked for helping with the sulfur isotope analysis. The editor, two anonymous reviewers and Professor Richard Stern (University of Alberta) are thanked for their insightful and detailed comments, which significantly enhanced the manuscript. This research was jointly supported by the National Key R&D Program of China (2018YFA0702600), the Guangzhou Municipal Government Fund (201607020029), the Chinese National Science Fund for Distinguished Young Scholars (41725009) and the National Natural Science Foundation for Young Scientists of China (41903010).

References

Barnes S.-J. and Lightfoot P.C. (2005)
Formation of magmatic nickel-sulfide ore deposits and processes affecting their copper and platinum-group element contents. **Economic Geology**, 179–213.

references

Batanova V.G., Thompson J.M., Danyushevsky L.V., Portnyagin M.V., Garbe-Schönberg D., Hauri E., Kimura J.I., Chang Q., Senda R., Goemann K., Chauvel C., Campillo S., Ionov D.A. and Sobolev A.V. (2019)
New olivine reference material for *in situ* microanalysis. Geostandards and Geoanalytical Research, 43, 453–473.

Bortnikov N., Genkin A., Dobrovol'Skaya M., Muravitskaya G. and Filimonova A. (1991)
The nature of chalcopyrite inclusions in sphalerite: Exsolution, coprecipitation, or "disease"? Economic Geology, 86, 1070–1082.

Bryant R.N., Jones C., Raven M.R., Gomes M.L., Berelson W.M., Bradley A.S. and Fike D.A. (2019)
Sulfur isotope analysis of microcrystalline iron sulfides using secondary ion mass spectrometry imaging: Extracting local paleo-environmental information from modern and ancient sediments. Rapid Communications in Mass Spectrometry, 33, 491–502.

Cabral R.A., Jackson M.G., Rose-Koga E.F., Koga K.T., Whitehouse M.J., Antonelli M.A., Farquhar J., Day J.M. and Hauri E.H. (2013)
Anomalous sulphur isotopes in plume lavas reveal deep mantle storage of Archaean crust. Nature, 496, 490–493.

Chen H.Y., Clark A.H., Kyser T.K., Ullrich T.D., Baxter R., Chen Y.M. and Moody T.C. (2010)
Evolution of the giant Marcona-Mina Justa iron oxide-copper-gold district, south-central Peru. Economic Geology, 105, 155–185.

Chen L., Chen K., Bao Z., Liang P., Sun T. and Yuan H. (2017)
Preparation of standards for *in situ* sulfur isotope measurement in sulfides using femtosecond laser ablation MC-ICP-MS. Journal of Analytical Atomic Spectrometry, 32, 107–116.

Chen L., Yuan H., Chen K., Bao Z., Zhu L. and Liang P. (2019)
In situ sulfur isotope analysis by laser ablation MC-ICP-MS and a case study of the Erlihe Zn-Pb ore deposit, Qinling orogenic belt, central China. Journal of Asian Earth Sciences, 176, 325–336.

Chen M., Campbell I.H., Xue Y., Tian W., Ireland T.R., Holden P., Cas R.A., Hayman P.C. and Das R. (2015)
Multiple sulfur isotope analyses support a magmatic model for the volcanogenic massive sulfide deposits of the Teutonic Bore Volcanic Complex, Yilgarn Craton, Western Australia. Economic Geology, 110, 1411–1423.

Crowe D.E. and Vaughan R.G. (1996)
Characterization and use of isotopically homogeneous standards for *in situ* laser microprobe analysis of S-34/S-32 ratios. American Mineralogist, 81, 187–193.

Cui H., Kitajima K., Spicuzza M.J., Fournelle J.H., Denny A., Ishida A., Zhang F. and Valley J.W. (2018)
Questioning the biogenicity of Neoproterozoic superheavy pyrite by SIMS. American Mineralogist, 103, 1362–1400.

Ding T., Valkiers S., Kipphardt H., De Bievre P., Taylor P.D.P., Gonfiantini R. and Krouse R. (2001)
Calibrated sulfur isotope abundance ratios of three IAEA sulfur isotope reference materials and V-CDT with a reassessment of the atomic weight of sulfur. Geochimica et Cosmochimica Acta, 65, 2433–2437.

Drake H., Åström M.E., Tullborg E.-L., Whitehouse M. and Fallick A.E. (2013)
Variability of sulphur isotope ratios in pyrite and dissolved sulphate in granitoid fractures down to 1 km depth – Evidence for widespread activity of sulphur reducing bacteria. Geochimica et Cosmochimica Acta, 102, 143–161.

Drake H., Whitehouse M.J., Heim C., Reiners P.W., Tillberg M., Hogmalm K.J., Dopson M., Broman C. and Åström M.E. (2018)
Unprecedented ^{34}S-enrichment of pyrite formed following microbial sulfate reduction in fractured crystalline rocks. Geobiology, 16, 556–574.

Eldridge C., Bourcier W., Ohmoto H. and Barnes H. (1988)
Hydrothermal inoculation and incubation of the chalcopyrite disease in sphalerite. Economic Geology, 83, 978–989.

Farquhar J., Bao H.M. and Thiemens M. (2000)
Atmospheric influence of Earth's earliest sulfur cycle. Science, 289, 756–758.

Farquhar J., Johnston D.T., Wing B.A., Habicht K.S., Canfield D.E., Airieau S. and Thiemens M.H. (2003)
Multiple sulphur isotopic interpretations of biosynthetic pathways: Implications for biological signatures in the sulphur isotope record. Geobiology, 1, 27–36.

Galley A.G., Hannington M.D. and Jonasson I. (2007)
Volcanogenic massive sulphide deposits: Mineral deposits of Canada: A synthesis of major deposit-types, district metallogeny, the evolution of geological provinces, and exploration methods: Geological Association of Canada, Mineral Deposits Division, Special Publication, 5, 141–161.

Gilbert S.E., Danyushevsky L.V., Rodemann T., Shimizu N., Gurenko A., Meffre S., Thomas H., Large R.R. and Death D. (2014)
Optimisation of laser parameters for the analysis of sulphur isotopes in sulphide minerals by laser ablation ICP-MS. Journal of Analytical Atomic Spectrometry, 29, 1042–1051.

Gu L., Zheng Y., Tang X., Zaw K., Della-Pasque F., Wu C., Tian Z., Lu J., Ni P., Li X., Yang F. and Wang X. (2007)
Copper, gold and silver enrichment in ore mylonites within massive sulphide orebodies at Hongtoushan VHMS deposit, N.E. China. Ore Geology Reviews, 30, 1–29.

Hartley M.E., Thordarson T., Taylor C., Fitton J.G. and Eimf (2012)
Evaluation of the effects of composition on instrumental mass fractionation during SIMS oxygen isotope analyses of glasses. Chemical Geology, 334, 312–323.

Hitzman M.W. and Valenta R.K. (2005)
Uranium in iron oxide-copper-gold (IOCG) systems. Economic Geology, 100, 1657–1661.

references

Ireland T.R., Schram N., Holden P., Lanc P., Ávila J., Armstrong R., Amelin Y., Latimore A., Corrigan D., Clement S., Foster J.J. and Compston W. (2014)
Charge-mode electrometer measurements of S-isotopic compositions on SHRIMP-SI. International Journal of Mass Spectrometry, 359, 26–37.

ISO Guide 35 (2017)
Reference materials – Guidance for characterization and assessment of homogeneity and stability. International Organization for Standardization (Geneva), 114pp.

Kita N.T., Ushikubo T., Fu B. and Valley J.W. (2009)
High precision SIMS oxygen isotope analysis and the effect of sample topography. Chemical Geology, 264, 43–57.

LaFlamme C., Martin L., Jeon H., Reddy S.M., Selvaraja V., Caruso S., Bui T.H., Roberts M.P., Voute F., Hagemann S., Wacey D., Littman S., Wing B., Fiorentini M. and Kilburn M.R. (2016)
In situ multiple sulfur isotope analysis by SIMS of pyrite, chalcopyrite, pyrrhotite, and pentlandite to refine magmatic ore genetic models. Chemical Geology, 444, 1–15.

Li R., Chen H., Xia X., Yang Q., Danyushevsky L.V. and Lai C. (2018)
Using integrated *in-situ* sulfide trace element geochemistry and sulfur isotopes to trace ore-forming fluids: Example from the Mina Justa IOCG deposit (southern Perú). Ore Geology Reviews, 101, 165–179.

Li R., Chen H., Xia X., Yang Q., Li L., Xu J., Huang C. and Danyushevsky L.V. (2017)
Ore fluid evolution in the giant Marcona Fe-(Cu) deposit, Perú: Evidence from *in-situ* sulfur isotope and trace element geochemistry of sulfides. Ore Geology Reviews, 86, 624–638.

Li R., Xia X., Yang S., Chen H. and Yang Q. (2019)
Off-mount calibration and one new potential pyrrhotite reference material for sulfur isotope measurement by secondary ion mass spectrometry. Geostandards and Geoanalytical Research, 43, 177–187.

Molnár F., Mänttäri I., O'Brien H., Lahaye Y., Pakkanen L., Johanson B., Käpyaho A., Sorjonen-Ward P., Whitehouse M. and Sakellaris G. (2016)
Boron, sulphur and copper isotope systematics in the orogenic gold deposits of the Archaean Hattu schist belt, eastern Finland. Ore Geology Reviews, 77, 133–162.

Ohmoto H. and Goldhaber M.B. (1997)
Sulfur and carbon isotopes. In: Barnes H.L. (ed.), Geochemistry of hydrothermal ore deposits. Wiley (New York), 517–611.

Ono S. (2017)
Photochemistry of sulfur dioxide and the origin of mass-independent isotope fractionation in Earth's atmosphere. Annual Review of Earth and Planetary Sciences, 45, 301–329.

Ono S., Shanks W.C., Rouxel O.J. and Rumble D. (2007)
S-33 constraints on the seawater sulfate contribution in modern seafloor hydrothermal vent sulfides. Geochimica et Cosmochimica Acta, 71, 1170–1182.

Othmane G., Hull S., Fayek M., Rouxel O., Lahd G.M. and Kyser T.K. (2015)
Hydrogen and copper isotope analysis of turquoise by SIMS: Calibration and matrix effects. Chemical Geology, 395, 41–49.

Paris G., Adkins J.F., Sessions A.L., Webb S.M. and Fischer W.W. (2014)
Neoarchean carbonate-associated sulfate records positive $\Delta^{33}S$ anomalies. Science, 346, 739–741.

Seal R.R. (2006)
Sulfur isotope geochemistry of sulfide minerals. Sulfide Mineralogy and Geochemistry, 61, 633–677.

Shen Y., Farquhar J., Masterson A., Kaufman A.J. and Buick R. (2009)
Evaluating the role of microbial sulfate reduction in the early Archean using quadruple isotope systematics. Earth and Planetary Science Letters, 279, 383–391.

Sillitoe R.H. (2010)
Porphyry copper systems. Economic Geology, 105, 3–41.

Ulrich T., Long D.G.F., Kamber B.S. and Whitehouse M.J. (2011)
In situ trace element and sulfur isotope analysis of pyrite in a Paleoproterozoic gold placer deposit, Pardo and Clement townships, Ontario, Canada. Economic Geology, 106, 667–686.

Ushikubo T., Williford K.H., Farquhar J., Johnston D.T., Van Kranendonk M.J. and Valley J.W. (2014)
Development of *in situ* sulfur four-isotope analysis with multiple Faraday cup detectors by SIMS and application to pyrite grains in a Paleoproterozoic glaciogenic sandstone. Chemical Geology, 383, 86–99.

Valley J.W. and Kita N.T. (2009)
In situ oxygen isotope geochemistry by ion microprobe. MAC Short Course: Secondary Ion Mass Spectrometry in the Earth sciences, 41, 19–63.

Wagner T., Okrusch M., Weyer S., Lorenz J., Lahaye Y., Taubald H. and Schmitt R.T. (2010)
The role of the Kupferschiefer in the formation of hydrothermal base metal mineralization in the Spessart ore district, Germany: Insight from detailed sulfur isotope studies. Mineralium Deposita, 45, 217–239.

Whitehouse M.J. (2013)
Multiple sulfur isotope determination by SIMS: Evaluation of reference sulfides for $\Delta^{33}S$ with observations and a case study on the determination of $\Delta^{36}S$. Geostandards and Geoanalytical Research, 37, 19–33.

Wu N., Farquhar J., Dottin J.W. and Magalhães N. (2018)
Sulfur isotope signatures of eucrites and diogenites. Geochimica et Cosmochimica Acta, 233, 1–13.

references

Zhang J., Lin Y., Yan J., Li J. and Yang W. (2017) Simultaneous determination of sulfur isotopes and trace elements in pyrite with a NanoSIMS 50L. **Analytical Methods**, **9**, 6653–6661.

Zhang J., Lin Y., Yang W., Shen W., Hao J., Hu S. and Cao M. (2014a) Improved precision and spatial resolution of sulfur isotope analysis using NanoSIMS. **Journal of Analytical Atomic Spectrometry**, **29**, 1934–1943.

Zhang Y., Sun F., Li B., Huo L. and Ma F. (2014b) Ore textures and remobilization mechanisms of the Hongtoushan copper–zinc deposit, Liaoning, China. **Ore Geology Reviews**, **57**, 78–86.

Zhu M.-T., Zhang L.-C., Dai Y.-P. and Wang C.-L. (2015) *In situ* zircon U-Pb dating and O isotopes of the Neoarchean Hongtoushan VMS Cu–Zn deposit in the North China Craton: Implication for the ore genesis. **Ore Geology Reviews**, **67**, 354–367.

Supporting information

The following supporting information may be found in the online version of this article:

Table S1. Original $^{34}S/^{32}S$ ratios of HTS4-6 chalcopyrite and *F*-test results.

Table S2. $\delta^{34}S$ values of HTS4-6 chalcopyrite determined using LA-MC-ICP-MS.

This material is available from: http://onlinelibrary.wiley.com/doi/10.1111/ggr.12330/abstract (This link will take you to the article abstract).